IEEE TRANSACTIONS ON

SUSTAINABLE ENERGY

IEEE POWER & ENERGY SOCIETY
IEEE POWER ELECTRONICS SOCIETY
IEEE INDUSTRY APPLICATIONS SOCIETY
IEEE INDUSTRIAL ELECTRONICS SOCIETY

TECHNICALLY COSPONSORED BY
IEEE SOCIETY ON SOCIAL IMPLICATIONS OF TECHNOLOGY
IEEE PHOTONICS SOCIETY
IEEE INSTRUMENTATION & MEASUREMENT SOCIETY

OCTOBER 2010 VOLUME 1 NUMBER 3 ITSEAJ (ISSN 1949-3029)

An Improved Control Strategy for Hybrid Wind Farms

Andres E. Leon, *Student Member, IEEE*, Juan Manuel Mauricio, *Student Member, IEEE*, Antonio Gómez-Expósito, *Fellow, IEEE*, and Jorge Alberto Solsona, *Senior Member, IEEE*

***Abstract*—This paper addresses the control requirements of hybrid wind farms, comprising a relatively large number of conventional induction machines (IMs) along with one or very few permanent magnet synchronous machines (PMSMs), capable of compensating the reactive power demanded by the IMs during faulty conditions as well as attenuating the active power variations due to wind gusts. Based on the superposition theorem and the feedback linearization technique, a controller is designed to independently regulate the positive and negative sequence currents of the PMSM voltage source converters (VSCs), overcoming several drawbacks of existing approaches in the presence of unbalanced voltages. In the proposed scheme, the grid-side VSC currents are controlled in order to improve the ride-through capability of IMs, so that the whole wind farm can fulfill demanding grid codes in the absence of extra equipment, such as static compensators. As shown by the test results, combining IM-based wind farms with PMSMs accomplishes several relevant goals: delivering the reactive power consumption of the IMs, increasing the rated active power of the installation, and smoothing mechanical power oscillations.**

***Index Terms*—Feedback linearization, grid codes, permanent magnet synchronous machines (PMSMs), unbalanced faults, voltage source converter (VSC), wind energy conversion system.**

NOMENCLATURE

Variables and parameters:

i_{ad}, i_{aq}	dq-axis machine-side voltage source converter (VSC) currents.
i_{bd}, i_{bq}	dq-axis grid-side VSC currents.
v_{bd}, v_{bq}	dq-axis B bus voltages.
$v_{\rm dc}$	DC-link voltage.
p_c	VSC instantaneous active power.
q_c	VSC instantaneous reactive power.
$p_{\rm IM}$	Induction machine (IM) instantaneous active power (all frequency spectrum).
$p_{\rm IM}^{\sim}$	High frequencies of the IM active power.
$q_{\rm IM}$	IM instantaneous reactive power.
$p_{\rm GOV}$	Active power from the permanent magnet synchronous machine (PMSM) speed governor.
ω_t, ω_r	Turbine and PMSM rotor speeds.
ω_s	Network angular frequency.
γ_{tr}	Angle between turbine and PMSM rotor.
η_{bd}, η_{bq}	dq control inputs of grid-side VSC.
T_t	Mechanical torque generated by the wind.
T_e	Electromagnetic torque.
Ψ_m	PMSM magnetic flux.
R_s	PMSM stator resistance.
L_s	PMSM stator self inductance.
R_a, R_b	Equivalent PMSM and grid-side VSC resistances.
L_a, L_b	PMSM and grid-side VSC coupling inductances.
R_s, R_r	IM stator and rotor resistances.
L_m	IM mutual inductance.
L_{ls}, L_{lr}	IM stator and rotor leakage inductances.
$C_{\rm dc}$	DC-link capacitance.
$N_{\rm gb}$	Gearbox ratio.
N_r	Number of PM rotor pair of poles.
H_t, H_r	Turbine and PMSM rotor inertia constants.
K_{tr}	Shaft stiffness.
D_{tr}	Shaft mutual damping.
D_{tb}, D_{rb}	Turbine and PMSM rotor mechanical dampings.
λ	Eigenvalue associated with the multimass turbine system.

Superscripts:

$+, -$	Positive and negative sequence.
$\star$	Desired reference value.

Manuscript received October 17, 2009; revised May 05, 2010; accepted August 05, 2010. Date of publication August 23, 2010; date of current version September 22, 2010. This work was supported by Universidad Nacional del Sur, Consejo Nacional de Investigaciones Científicas y Técnicas (CONICET) and Agencia Nacional de Promoción Científica y Tecnológica (ANPCyT), Argentina, and by the Spanish Ministry of Education and Science (MEC) and Junta de Andalucía under Grant ENE-2007-68032-C04-02 and Grant TEP-5170, respectively.

A. E. Leon and J. A. Solsona are with Instituto de Investigaciones en Ingeniería Eléctrica (IIIE) "Alfredo Desages" (UNS-CONICET), Departamento de Ingeniería Eléctrica y de Computadoras, Universidad Nacional del Sur (UNS), Bahía Blanca 8000, Argentina (e-mail: aleon@ymail.com; jsolsona@uns.edu.ar).

J. M. Mauricio and A. Gómez-Expósito are with the Department of Electrical Engineering, University of Seville, 41092 Seville, Spain (e-mail: j.m.mauricio@ieee.org; age@us.es).

Digital Object Identifier 10.1109/TSTE.2010.2068580

Subscripts:

α, β α- and β-axis component.

d, q d- and q-axis component.

I. Introduction

THE increasingly widespread use of wind generation in power networks imposes the requirement for wind farms to be capable of contributing to network support and operation, much in the same way as conventional synchronous generators are [1].

One of the most difficult requirements to meet for wind turbine generators is the capability to ride through a fault [2]–[4]. Traditionally, wind turbine generators were tripped once the voltage at their terminals reduced below 80%; that was acceptable because their impact on the grid was low. However, with ever-increasing penetration of wind energy, grid codes now generally demand higher performance of connected plants with respect to fault ride-through and power control capability [5], at voltages of 15% or less.

Fixed-speed IM-based wind energy conversion systems (IM-WECS) were common in the 1980s and 1990s when the wind energy production was almost negligible. These machines are not capable of controlling their reactive power consumption and have a very low ride-through capability. Therefore, they are becoming obsolete in power systems like the Spanish one, where grid codes are very restrictive. However, as roughly between 20% and 30% of wind energy in Spain still comes from IMs, technical solutions must be devised in order to assure that current wind farms agree with grid codes for their entire lifetime. The most frequent approach is based on shunt STATic COMpensators (STATCOM) [6] or series dynamic voltage restorers (DVRs) [7]. But this sort of solution, apart from taking advantage of the required investment only during a fault, does not increase the steady-state active power capacity of the wind farm.

The new generation of WECS based on permanent magnet synchronous machines (PMSMs) or double fed induction machines (DFIMs) are capable of controlling its active and reactive power outputs rapidly, as well as supporting nearby induction generators [8]. As the VSCs of PMSM-WECS, unlike those of DFIMs, are fully rated, in this work a PMSM-WECS is considered for compensating the IM-WECS reactive power consumption and averaging the active power variations due to wind gusts. This alternative can be profitable because, in addition to those transient functions, the required investment is used in steady state to increase the total injected energy.

At least two situations in which a hybridization between IMs and PMSMs could be of interest for WECS can be identified, namely:

1) Existing IM-based WECS, that must be uprated and/or upgraded to cope with more exigent grid codes. This is currently the case of Spain, where existing IM-WECS have to be either preserved by adding STATCOMs, DVRs, etc., or sold off to countries with less demanding grid-codes. Our proposal resorts to a strategy that can help in this situation in order to maintain, whenever possible, the current generation of IM-WECS.
2) New wind farm installations. The IM-WECS are simpler and cheaper than their variable speed counterparts because they do not involve power electronics. With the proposed hybridization, it would be possible to develop new wind farm designs based on a mix of IMs and PMSMs. Our tests below show that, with a PMSM-to-IM power ratio of around 2, it is possible to fully compensate the entire wind farm without demanding considerable over-currents from the PMSM converters. If an overload is transiently allowed (as commonly advertised by converter manufacturers), it is possible to have even a smaller power ratio.

In order to investigate the feasibility of improving the ride-through capability and the active power smoothness of IM-WECS by incorporating a PMSM-WECS, the control strategy is focused on the grid-side VSC, which is exposed to both balanced and unbalanced electric network faults. Most of the VSC controllers under unbalanced conditions can be classified in two categories. The first one, based on a dual sequence control (DSC) scheme [9]–[14], independently controls the positive and negative sequences using two reference frames rotating at synchronous speed, but in opposite directions. The second category of methods uses Proportional plus Resonant (PR) controllers [15]–[18], which allow tracking, without steady-state error, constant and sinusoidal current references arising in synchronous frames under unbalanced conditions. In several PMSM-WECS control approaches [19]–[24], the unbalanced conditions in the electric network are not taken into account. In order to improve the performance of PMSM-WECS applications, in [25] and [26], the same strategies are presented, considering that the grid-side VSC is connected to an unbalanced voltage. However, these works deal only with the dc-link voltage control and an arbitrary injection of power to the grid.

In this paper, a thorough analysis is presented related to how an IM-WECS can meet the grid code requirements through the inclusion of a PMSM-WECS. The active and reactive power references to be injected by the grid-side VSC are designed so that the whole wind farm, composed of both sorts of machines, can meet the current grid codes. Besides, the grid-side VSC control for tracking these power references is tailored for overcoming balanced and unbalanced faults which can arise in the electric network. To this end, the DSC scheme is chosen in the grid-side VSC controller design. The inclusion of the PMSM, along with its back-to-back converter, can enlarge the active power capacity of existing farms while providing the reactive power support during network faults and smoothing the active power output when wind gusts occurs.

The rest of the paper is organized as follows: Section II presents the PMSM and VSC models; the control strategy and the proposed operation philosophy are described in Sections III and IV, while performance tests, discussions, and results are shown in Section V. Finally, conclusions are given in Section VI.

II. PMSM-WECS Model

The PMSM-WECS considered in this work is schematically represented in Fig. 1. It comprises a wind turbine connected through a nonrigid shaft to the generator rotor. Other major components are the back-to-back VSCs through which the full

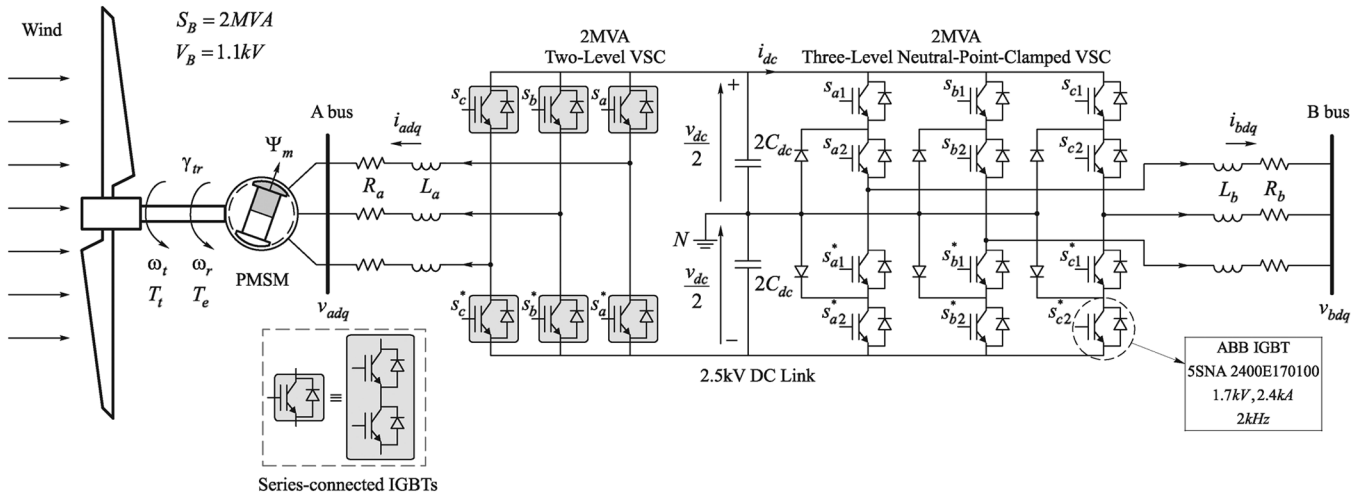

Fig. 1. PMSM-based wind energy system.

power of the PMSM-WECS is evacuated to the grid. Each device in this system will be explained in more detail below.

A. Electrical PMSM Model

In a synchronously rotating reference frame, the equations in p.u. describing the PMSM stator are [20] as follows:

$$L_{sd}\dot{i}_{sd} = -R_s i_{sd} - N_r\omega_r L_{sq} i_{sq} - v_{sd} \quad (1)$$

$$L_{sq}\dot{i}_{sq} = -R_s i_{sq} + N_r\omega_r L_{sd} i_{sd} + N_r\omega_r \Psi_m - v_{sq}. \quad (2)$$

B. Wind Turbine Mechanical System

The aim of this work is to control the active and reactive powers provided by the WECS from a transient point of view, for which it is important to model the mechanical subsystem. A two-mass lumped model is used to represent the mechanical dynamics (see Fig. 2), as proposed in [27] and [28]

$$2H_r\dot{\omega}_r = K_{tr}\gamma_{tr} - T_e + D_{tr}(\omega_t - \omega_r) - D_{rb}\omega_r \quad (3)$$

$$2H_t\dot{\omega}_t = T_t - K_{tr}\gamma_{tr} - D_{tr}(\omega_t - \omega_r) - D_{tb}\omega_t \quad (4)$$

$$\dot{\gamma}_{tr} = \Omega_B(\omega_t - \omega_r) \quad (5)$$

where

$$T_e = \frac{3}{2}\left(i_{sq}\Psi_m - (L_{sq} - L_{sd})i_{sd}i_{sq}\right). \quad (6)$$

C. PMSM-Side VSC Model

The machine-side converter is a two-level VSC connected through a filter to the PMSM stator. This converter controls the stator currents and the dc-link voltage, as described in the control strategy section below.

D. Grid-Side VSC Model

The grid-side converter is a three-level neutral-point-clamped VSC [29] connected through a step-up transformer to the grid.

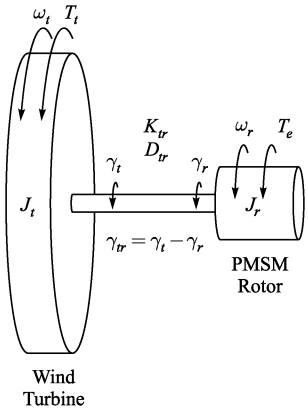

Fig. 2. Mechanical subsystem of the WECS consisting of two lumped masses (the wind turbine and the electric rotor) connected through a nonrigid shaft.

As a majority of faults in the electrical network are asymmetrical, it is necessary to develop models and controllers capable of facing the VSC connection to unbalanced voltages, as described below. The VSC model in the $\alpha-\beta$ stationary reference frame is given by [30]

$$L_b\dot{i}_{b\alpha} = -R_b i_{b\alpha} + e_{b\alpha} - v_{b\alpha} \quad (7)$$

$$L_b\dot{i}_{b\beta} = -R_b i_{b\beta} + e_{b\beta} - v_{b\beta} \quad (8)$$

where the VSC internal voltages have been defined as

$$e_{b\alpha} \triangleq \eta_{b\alpha} v_{\rm dc} \quad (9)$$

$$e_{b\beta} \triangleq \eta_{b\beta} v_{\rm dc}. \quad (10)$$

The equations describing the VSC are nonlinear owing to the presence of products like $\eta_b v_{\rm dc}$. The change of variables (9) and (10) leads to the linear system (7), (8). Therefore, assuming identical parameters for each phase, the superposition theorem can be applied [31].

Next, two transformations are defined. One of them, $\mathbf{A}(\theta)$, rotates at the network angular speed in the same direction as

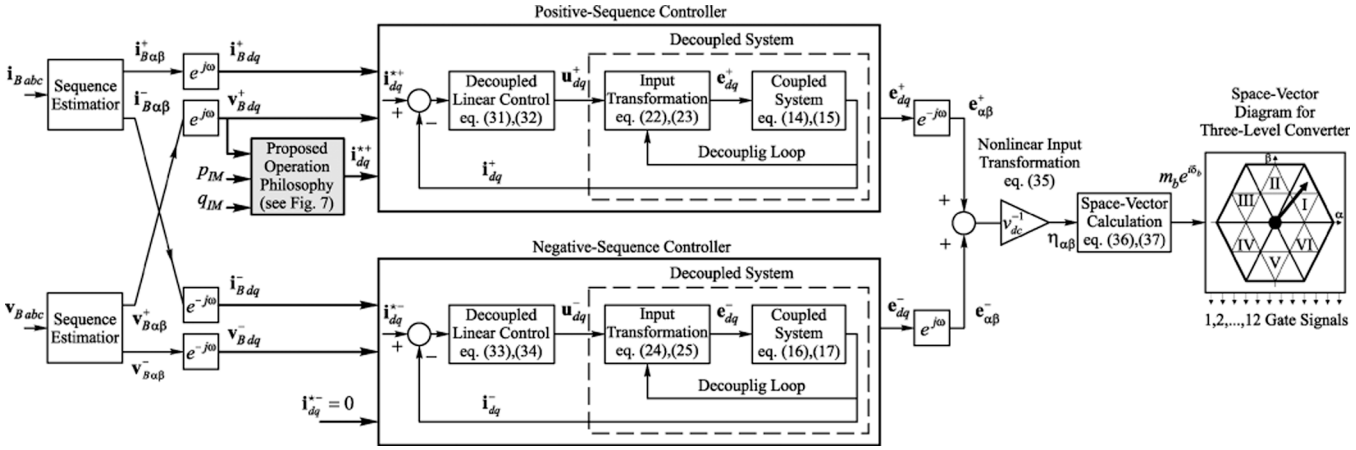

Fig. 3. Block diagram of the grid-side VSC control strategy.

the positive sequence components. The other, $\mathbf{A}(-\theta)$, also rotates at the network angular speed but in the opposite direction. Therefore, for a generic vector $\mathbf{x}_{\alpha\beta}$, it can be written

$$\mathbf{x}_{dq}^{+} = \mathbf{A}(\theta)\mathbf{x}_{\alpha\beta}^{+} \tag{11}$$

$$\mathbf{x}_{dq}^{-} = \mathbf{A}(-\theta)\mathbf{x}_{\alpha\beta}^{-} \tag{12}$$

where $\theta = \omega_s t$ and

$$\mathbf{A}(\theta) = \begin{bmatrix} \cos\theta & -\sin\theta \\ \sin\theta & \cos\theta \end{bmatrix}. \tag{13}$$

These transformations define two reference frames, $d-q^{+}$ and $d-q^{-}$, in which rotating components of positive and negative sequence, respectively, are seen as constant signals. This way, it is possible to implement two independent control loops, one for each sequence in the respective reference frame, which can be easily tuned.

Finally, applying the transformations (11) and (12) to the VSC model (7), (8), in the $\alpha\beta^{+}$ and $\alpha\beta^{-}$ stationary reference frames, yields [32]

$$L_b \dot{i}_{bd}^{+} = -R_b i_{bd}^{+} - L_b \omega_s i_{bq}^{+} + e_{bd}^{+} - v_{bd}^{+} \tag{14}$$

$$L_b \dot{i}_{bq}^{+} = -R_b i_{bq}^{+} + L_b \omega_s i_{bd}^{+} + e_{bq}^{+} - v_{bq}^{+} \tag{15}$$

$$L_b \dot{i}_{bd}^{-} = -R_b i_{bd}^{-} + L_b \omega_s i_{bq}^{-} + e_{bd}^{-} - v_{bd}^{-} \tag{16}$$

$$L_b \dot{i}_{bq}^{-} = -R_b i_{bq}^{-} - L_b \omega_s i_{bd}^{-} + e_{bq}^{-} - v_{bq}^{-}. \tag{17}$$

The above equations will be used in Section III in order to develop the control strategy under unbalanced conditions.

III. Control Strategy

The control strategy can be divided in two blocks. On the one hand, the management of the active and reactive power injected by the PMSM is achieved by the grid-side VSC. On the other hand, the stator current control of the PMSM along with the dc-link regulation are accomplished by the machine-side VSC.

A. Grid-Side VSC Control

The dynamic model (14)–(17) obtained in the above section for the grid-side VSC can be split in two subsystems, namely (14), (15) and (16), (17), in the $d-q^{+}$ and $d-q^{-}$ reference frames, respectively. As both subsystems are decoupled, independent control strategies can be designed for each one. This idea is known in the literature as dual sequence control (DSC). A block diagram of the whole grid-side VSC control strategy is shown in Fig. 3, the details of which are provided in the Appendix.

B. Machine-Side VSC Control

The $d-q$ control applied to the machine-side VSC is synchronized with the d-axis (aligned with the PMSM magnetic flux). Therefore, the reference current $i_{ad}^{\star}$ is set to zero in order to avoid demagnetization, while the i_{aq} current is used to regulate the dc-link voltage. This approach is different from the more common one, where the grid-side VSC is used to control the dc-link voltage. With the proposed strategy a more accurate control of grid injected powers can be achieved, allowing the grid-side VSC to control its active and reactive powers in order to comply with the grid code requirements in a better way. A feedforward term from the active power injected by the grid-side VSC is included to minimize the dc voltage variations when active power transients occur [33].

Fig. 4 provides the block diagram of the PMSM-side VSC control strategy. In the first stage, the active power is calculated via a PI controller from the dc-link voltage regulator. The second stage introduces the feedforward term and transforms the power signals into current references. In the last stage, the current control loop and the space-vector modulation determines the PMSM-side VSC gate signals.

IV. Proposed Operation Philosophy

The inclusion of a PMSM within a conventional IM-based farm provides several advantages for both the farm itself and the electrical network. Some of them are:

1) compensating the reactive power demanded by an IM-WECS during three-phase and unbalanced faults;
2) averaging active power variations due to wind gusts;
3) improving the low voltage ride-through capability of nearby IM-WECS;
4) allowing the kinetic energy stored by rotational masses to be transiently released in order to provide earlier frequency support;

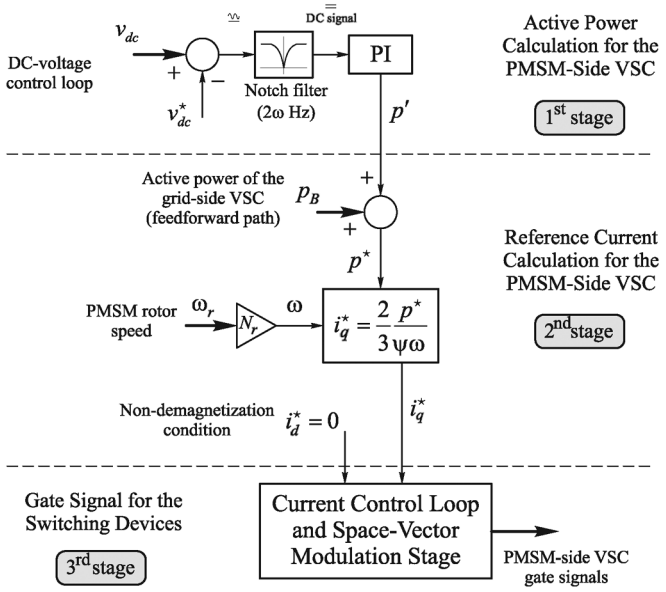

Fig. 4. Block diagram of the PMSM-side VSC control strategy.

5) enhancing the ability of the whole wind farm to fulfill increasingly demanding grid codes;
6) improving the WECS dynamic response (for example, power oscillation damping [34], [35], voltage stability [36], etc.);
7) enhancing the nominal active power capacity of the whole wind farm.

Some of these issues are discussed below, along with the proposed operation philosophy in order to calculate the grid-side VSC currents.

As mentioned at the introduction, grid codes now generally demand continued operation when the voltage drops to 15% of its rated value, or even lower. In Fig. 5, the grid code requirements imposed by some European countries are shown. The plot shows general shapes of voltage tolerance that most grid operators demand. Tripping is not allowed during and after a fault causing a voltage drop with a magnitude and duration above the curve. As can be observed, there is no harmonization in the grid codes, even among countries of the European Union. In this work, the voltage sag considered is a mix between that imposed by Germany and Spain, by far the largest wind energy producers in Europe. The voltage sag considered in Germany comprises an interval of 150 ms with 0 pu voltage. This requires the use of quick measurement and synchronization systems, capable of recovering their synchronism after the 0 pu condition. Furthermore, with null voltage, it is impossible to inject active power, which causes an important acceleration of all machines. On the other hand, the Spanish grid code considers a 20% voltage level lasting for 500 ms. This interval is long enough to make the IM-WECS slip over 7%, in spite of fast pitch angle controllers being used. Therefore, the considered voltage sag basically has a 150-ms interval with 0 pu voltage followed by another interval of 350 ms with 0.2 pu. The rest of the sag profile is shown in Fig. 6(a).

Also, a reactive current in proportion to the voltage drop may have to be provided, during and immediately after the fault, for

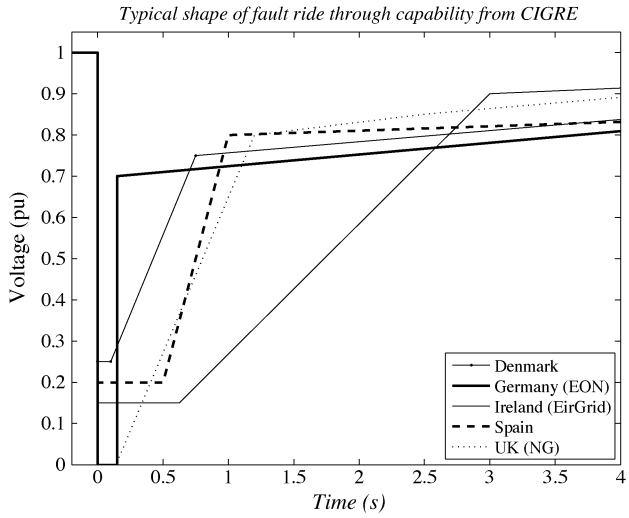

Fig. 5. Typical shape of fault ride-through capability, taken from [2].

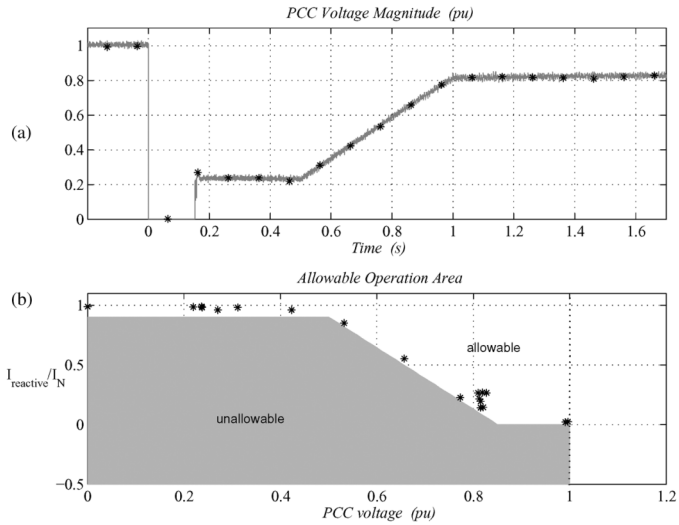

Fig. 6. Voltage sag profile and grid code requirement for reactive network support.

the purpose of voltage support and to enable coordination with the protection system [37]. The injected reactive current versus the PCC voltage level is shown in Fig. 6(b). The area outside the shaded polygon indicates the allowable operation area where the WECS has to work during voltage sags, according to the Spanish grid code [38].

In the steady state, the grid-side VSC regulates the PMSM rotor speed through the active power control. This regulation is quite slow, as it depends on mechanical time constants. Therefore, during a fast electrical transient, like a fault, the speed regulation can be momentarily neglected and both the active and reactive powers can be changed rather arbitrarily for other purposes, for example to support the grid during a voltage sag.

When a fault occurs, the grid-side VSC can transiently inject its nominal reactive power in order to support the reactive power requirements of nearby IM-WECS. At the same time, a momentary increase in the PMSM rotor speed takes place. As shown below, this support may be sufficient to guarantee that both kinds of WECS, when considered as a whole, satisfy the

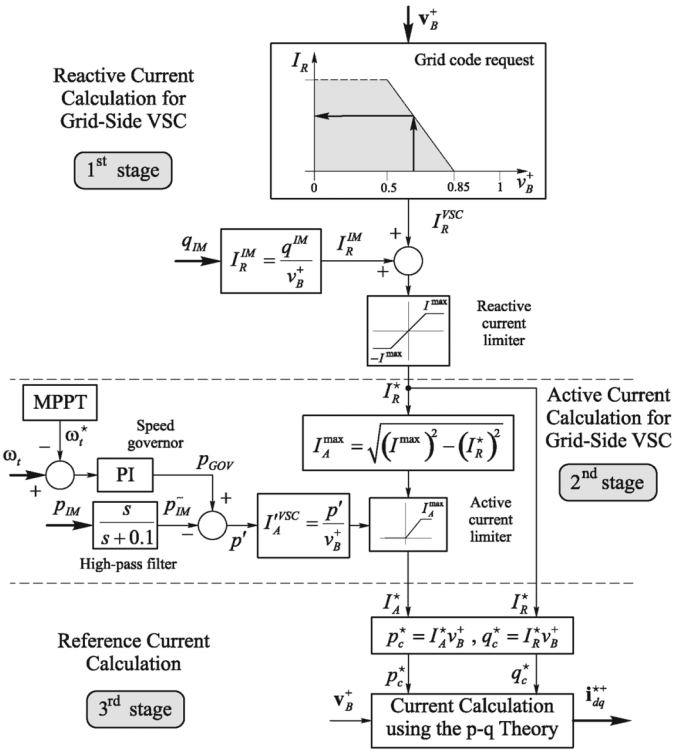

Fig. 7. Simplified scheme of grid-side VSC reference current calculation.

strong requirement currently demanded by the network operator.

Finally, when a sudden wind gust hits an IM-WECS, a transient variation in both the active and reactive power injected to the grid occurs. In order for the electrical network to receive a power as constant as possible, the kinetic energy stored by rotational masses of the PMSM-WECS can be used to smooth the active power injected to the grid by the whole wind farm.

Based on the above considerations, a control strategy is proposed to determine the current references to be injected by the grid-side VSC in order for the whole wind farm to improve its performance and fulfill the current grid codes. Fig. 7 shows a simplified diagram of the proposed reference current calculation method, composed of three blocks. In the first stage, the reactive current component (I_R^{VSC}) is obtained by using the WECS allowable operation area (see the bottom subplot of Fig. 6). Then, the reactive current absorbed by the IM-WECS (I_R^{IM}) is added to the grid-side VSC current. In this way, the reactive power consumed by the IM is not seen at the PCC. In the second stage, the sudden variations of the IM-WECS active power are extracted, using a high-pass filter designed to keep only the higher frequencies components. The resulting time-varying signal $(p_{\mathrm{IM}}^{\sim})$ is added with opposite sign to the grid-side VSC reference, in order to minimize the effect of wind gusts. This stage also takes into account the slower active power loop from the PMSM speed governor, which is denoted as p_{GOV}. The speed governor tracks the optimal turbine speed $(\omega_t^{\star})$ which is obtained from the maximum power point tracking (MPPT) algorithm. A description of this technique is presented in [39]–[41]. Then, the reference currents are limited for the sake of switching power devices protection. Finally, in the third stage, the above active and reactive components are transformed into the correct $d-q$ current reference frame by using the instantaneous power $p-q$ theory [42].

V. Performance Testing

This section presents the most relevant results regarding the assessment of the proposed control strategy. The PMSM, IMs, VSCs and control strategy are implemented via realistic models (discrete switching devices) by using the SimPowerSystems blockset of MATLAB. The power system configuration and parameters used in these tests are shown in Fig. 8.

A. Solid Two-Phase-to-Ground Fault Test

In order to test the behavior of the proposed controller and the grid-side VSC under unbalanced conditions, a 500-ms two-phase-to-ground fault is simulated at the WECS point of common coupling (PCC). Fig. 9(a) shows the PCC bus voltage when the asymmetrical fault begins. In Fig. 9(b), it can be seen that, in spite of the VSC being connected to a bus with a highly unbalanced voltage, the currents injected by the grid-side VSC are perfectly balanced.

In Fig. 10(a), the active and reactive powers injected by the whole WECS to the network are drawn. As can be observed, the capacitive reactive power injected during the fault allows the WECS to satisfy the specifications of wind farm regulations. Finally, Fig. 10(b) shows that the dc-link voltage excursions, including the characteristic double frequency ripple, are sufficiently small, both at the beginning and the end of the fault period.

B. Three-Phase Fault Test

Usually, the three-phase fault is the most demanding one in a power system. The considered control strategy is tested when the reactive power absorbed by the IM-WECS is compensated while maintaining the correct behavior of the PMSM.

Fig. 11(a) shows the active power output of the IM-WECS in this case. This power depends on the machine terminal voltage, which is considerably low during the fault [see Fig. 6(a)]. The active power contributed by the PMSM can be observed in Fig. 11(b). As explained in Section III, the priority in most grid codes is to follow a determined reactive power reference. Therefore, the active power of the PMSM is set to zero during most of the fault interval, in order to maximize the amount of reactive power that can be injected without overloading the involved devices. Indeed, the capability of any device to inject active power during very low terminal voltage conditions is quite limited. The total active power injected by both machines at the PCC is shown in Fig. 11(c).

The IM-WECS reactive power response is given in Fig. 12(a). As can be expected for such a long standing fault, the demanded reactive power when the voltage starts to recover can reach twice the nominal power. This is one of the reasons why a 2-MW PMSM is selected to compensate a 1-MW IM-WECS. If an important overcurrent is permitted in the PMSM, larger IM-WECSs can be considered. Fig. 12(b) shows the controlled reactive power provided by the PMSM. The response is fast and accurate, following the reference obtained from the algorithm summarized in Fig. 7. Fig. 12(c) represents the total reactive power at the PCC. As can be observed, the reactive power is

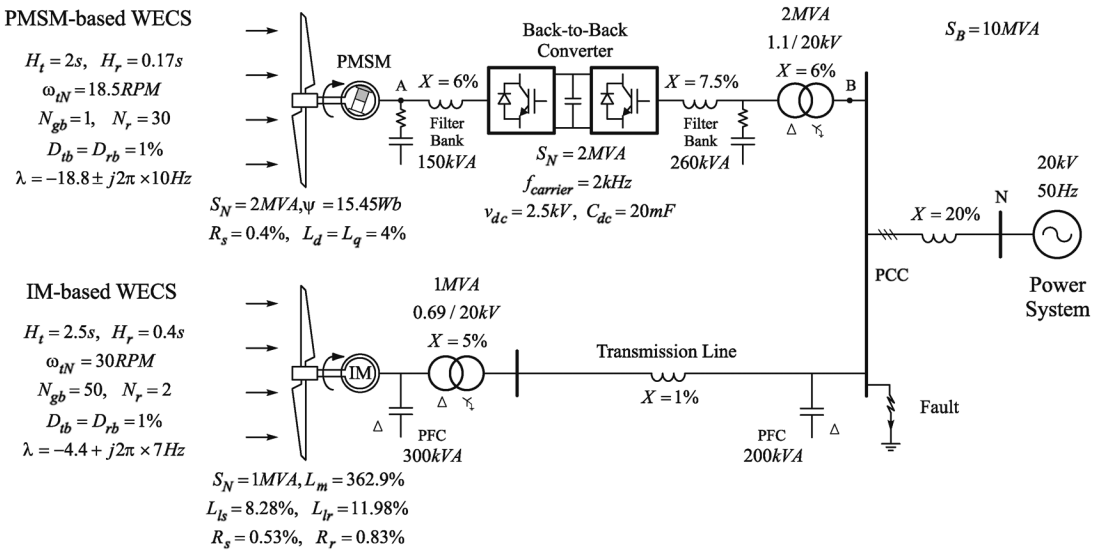

Fig. 8. Power system configuration and parameters used in the tests.

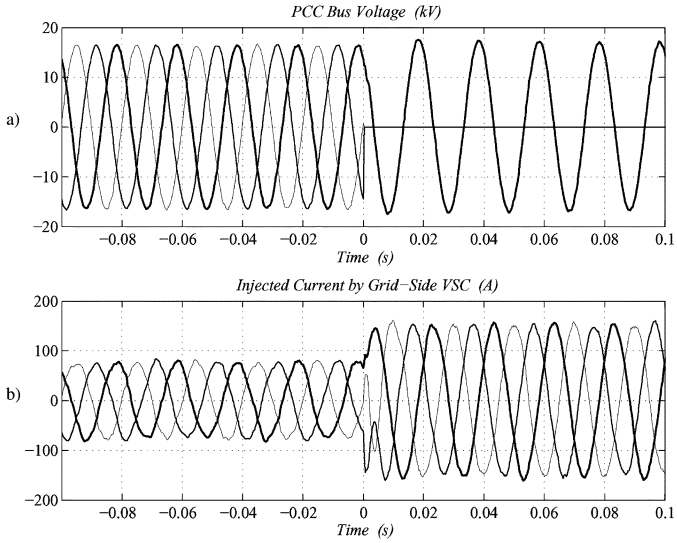

Fig. 9. Waveforms of PCC voltages and injected current by the grid-side VSC during the asymmetrical fault inception.

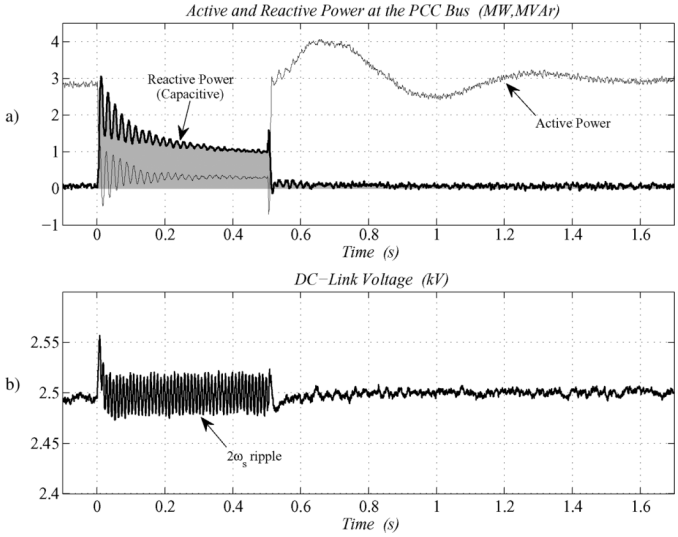

Fig. 10. Active and reactive power at the PCC bus, and dc-link voltage regulation during the asymmetrical fault.

always positive (capacitive) during the fault. Immediately after the fault, a certain level of reactive power is still injected to the grid, as required by the grid code, since the PCC voltage remains under 0.85 pu.

The reader is referred back to Fig. 6(a), in which the profile of the PCC voltage magnitude throughout the period of interest is represented with star marks. The same marks are also added to the bottom subplot of Fig. 6, clearly showing that the whole farm, composed of the PMSM- and the IM-WECS, remains in the allowed operating area when the proposed strategy is adopted.

Finally, Figs. 13(a) and (b) show, respectively, the PMSM and the IM mechanical speeds, for both the turbine and the rotor. As expected, the PMSM speed grows during the fault, since the injected active power is null to maximize the reactive power support. After the fault, however, the PMSM speed gradually returns to the initial value (not shown in the figure). Also, the dc-link voltage is depicted in Fig. 13(c), where it can be seen that the proposed strategy provides a good regulation.

C. Wind Gust Test

This test is aimed at showing the performance of the proposed strategy against wind gusts and its capacity to smooth power variations. Fig. 14(a) presents the wind gust model for this experiment, taken from [43]. The next figures show the active and reactive power injected to the grid during the disturbance, as follows: (b) by the IM-WECS only; (c) by the whole wind farm (IM- and PMSM-WECS) when the PMSM is independently controlled in absence of the proposed controller; (d) by the whole WECS when the proposed scheme is implemented. Note that both the active and reactive powers are considerably smoothed thanks to the coordinated controller presented in Figs. 3 and 7. Finally, Fig. 14(e) shows the PMSM rotor speed when the PMSM-WECS is smoothing the active

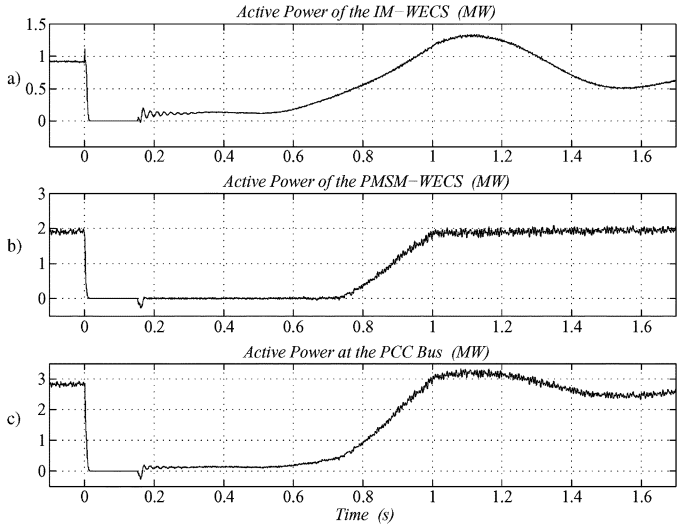

Fig. 11. Active power at the PCC bus during a three-phase fault.

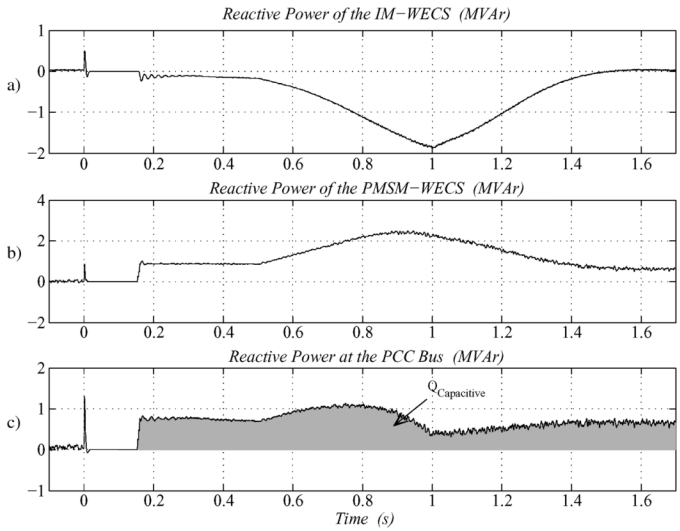

Fig. 12. Reactive power at the PCC bus during a three-phase fault.

power. A rotor speed variation is observed due to the PMSM conversion of wind kinetic energy into active power. However, these speed variations are under normal operation values.

VI. Conclusions

An alternative to the classic solution based on STATCOMs was presented, in order to improve the performance of IM-WECS. The idea is to complement existing IM-WECS with PMSM-WECS and then to control the total injected current in an appropriate and coordinated manner. The proposed control strategy determines the current references of the grid-side VSC, allowing the reactive power consumed by the IM to be compensated in such a way that the fault ride-through requirements of today's exigent grid codes are fulfilled. Also, the oscillations of active power injected to the grid, originated for instance by wind gusts, can be significantly smoothed by resorting to the kinetic energy stored in the PMSM mechanical system. The design of the control scheme faces both balanced and unbalanced faults, occurring in the electrical network. Several scenarios

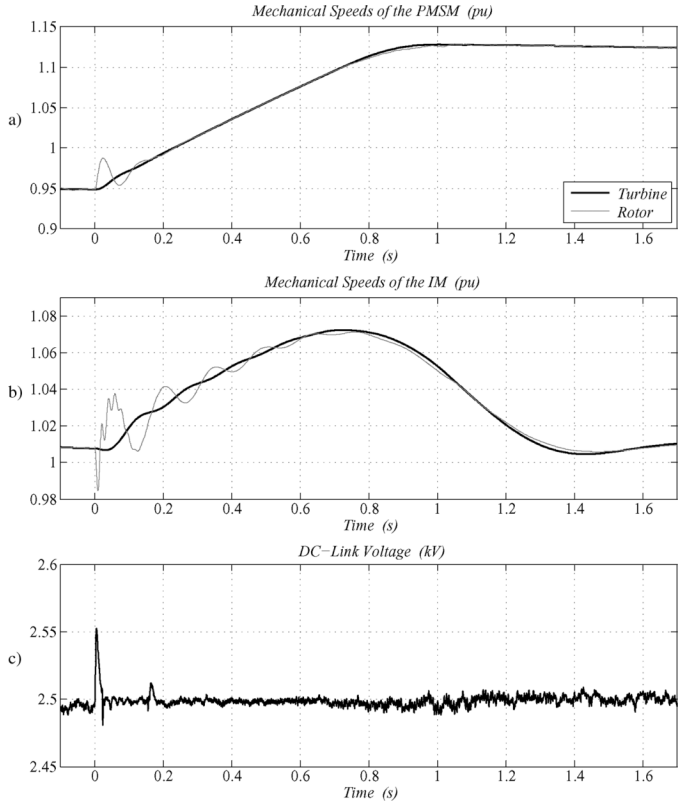

Fig. 13. PMSM and IM speed responses during a three-phase fault.

and disturbances, carefully chosen to provide a realistic assessment, have been tested showing the adequacy of the proposed arrangement and controllers, which can be an attractive choice for current IM-WECS in view of the ever-increasing grid code requirements.

Appendix

Taking into account (18)–(21), which are obtained from (14)–(17), the auxiliary control inputs u_{bd}^{+}, u_{bq}^{+}, u_{bd}^{-}, and u_{bq}^{-} are defined, allowing a direct and decoupled control of the currents injected to the network by the grid-side VSC

$$\dot{i}_{bd}^{+} = -\frac{R_b}{L_b} i_{bd}^{+} - \omega_s i_{bq}^{+} + \frac{e_{bd}^{+} - v_{bd}^{+}}{L_b} \triangleq u_{bd}^{+} \tag{18}$$

$$\dot{i}_{bq}^{+} = -\frac{R_b}{L_b} i_{bq}^{+} + \omega_s i_{bd}^{+} + \frac{e_{bq}^{+} - v_{bq}^{+}}{L_b} \triangleq u_{bq}^{+} \tag{19}$$

$$\dot{i}_{bd}^{-} = -\frac{R_b}{L_b} i_{bd}^{-} + \omega_s i_{bq}^{-} + \frac{e_{bd}^{-} - v_{bd}^{-}}{L_b} \triangleq u_{bd}^{-} \tag{20}$$

$$\dot{i}_{bq}^{-} = -\frac{R_b}{L_b} i_{bq}^{-} - \omega_s i_{bd}^{-} + \frac{e_{bq}^{-} - v_{bq}^{-}}{L_b} \triangleq u_{bq}^{-}. \tag{21}$$

From (18)–(21), the internal voltages of the grid-side VSC are obtained as

$$e_{bd}^{+} = R_b i_{bd}^{+} + L_b \omega_s i_{bq}^{+} + v_{bd}^{+} + L_b u_{bd}^{+} \tag{22}$$

$$e_{bq}^{+} = R_b i_{bq}^{+} - L_b \omega_s i_{bd}^{+} + v_{bq}^{+} + L_b u_{bq}^{+} \tag{23}$$

$$e_{bd}^{-} = R_b i_{bd}^{-} - L_b \omega_s i_{bq}^{-} + v_{bd}^{-} + L_b u_{bd}^{-} \tag{24}$$

$$e_{bq}^{-} = R_b i_{bq}^{-} + L_b \omega_s i_{bd}^{-} + v_{bq}^{-} + L_b u_{bq}^{-}. \tag{25}$$

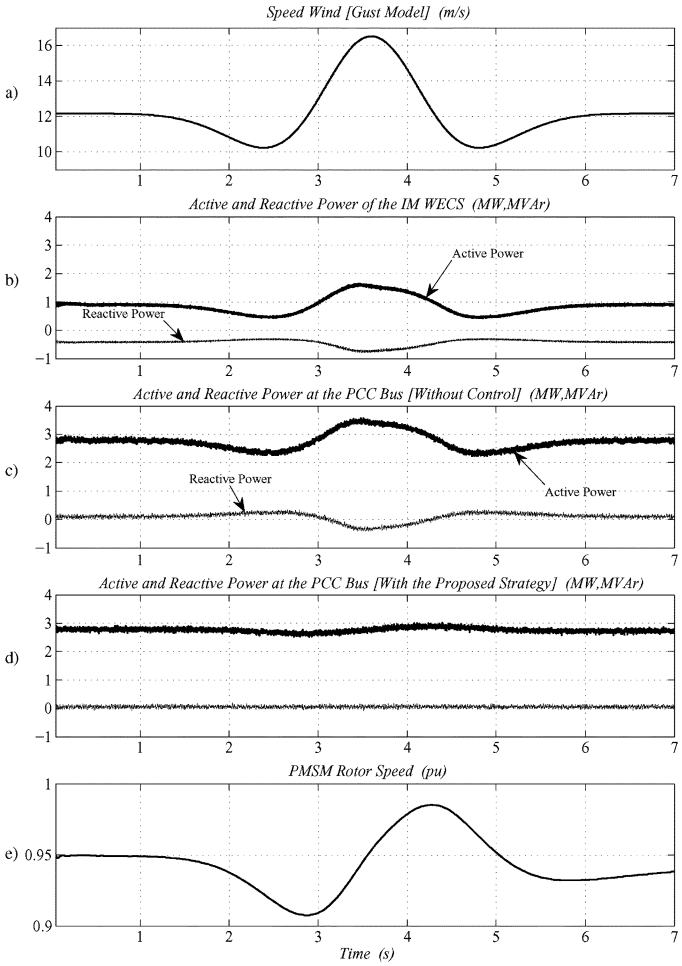

Fig. 14. Wind gust test to assess the controller capacity of smoothing the active power injected at the PCC.

In this way, by applying the input transformations (22)–(25), the transformed system becomes a decoupled linear system, (26)–(29), the states of which are time constants

$$\dot{i}_{bd}^{+} = u_{bd}^{+} \tag{26}$$
$$\dot{i}_{bq}^{+} = u_{bq}^{+} \tag{27}$$
$$\dot{i}_{bd}^{-} = u_{bd}^{-} \tag{28}$$
$$\dot{i}_{bq}^{-} = u_{bq}^{-}. \tag{29}$$

Note that the system (26)–(29) has a structure of the general form $\dot{i} = u$. Since the relative degree of i is one, a first-order tracking error dynamics is chosen, $\dot{\tilde{i}} + k\tilde{i} = 0$, where the current tracking error is defined as $\tilde{i} \triangleq i - i^{\star}$. From this error dynamic equation the auxiliary input u can be obtained as

$$u = \dot{i}^{\star} - k(i - i^{\star}). \tag{30}$$

As (30) represents a linear dynamics, linear techniques can be applied in order to determine the constant k. In this work, the pole placement technique is used, where the pole is chosen as a trade-off between the amplification of the PWM noise in the current measurement and the bandwidth of the controller, yielding $k = 900$.

Then, the four auxiliary control inputs u_{bd}^{+}, u_{bq}^{+}, u_{bd}^{-}, and u_{bq}^{-} can be obtained from the general expression (30) leading to

$$u_{bd}^{+} = \dot{i}_{bd}^{+\star} - k\left(i_{bd}^{+} - i_{bd}^{+\star}\right) \tag{31}$$
$$u_{bq}^{+} = \dot{i}_{bq}^{+\star} - k\left(i_{bq}^{+} - i_{bq}^{+\star}\right) \tag{32}$$
$$u_{bd}^{-} = \dot{i}_{bd}^{-\star} - k\left(i_{bd}^{-} - i_{bd}^{-\star}\right) \tag{33}$$
$$u_{bq}^{-} = \dot{i}_{bq}^{-\star} - k\left(i_{bq}^{-} - i_{bq}^{-\star}\right). \tag{34}$$

Finally, the control inputs $\eta_{b\alpha}$ and $\eta_{b\beta}$ are obtained from (9) and (10), using (22)–(25), yielding

$$\begin{bmatrix}\eta_{b\alpha}\\ \eta_{b\beta}\end{bmatrix} = \frac{1}{v_{\mathrm{dc}}}\left(\mathbf{A}^{-1}(\theta)\begin{bmatrix}e_{bd}^{+}\\ e_{bq}^{+}\end{bmatrix} + \mathbf{A}^{-1}(-\theta)\begin{bmatrix}e_{bd}^{-}\\ e_{bq}^{-}\end{bmatrix}\right). \tag{35}$$

The actual driving signals for the VSC are obtained with a pulsewidth modulator (PWM) with inputs $\eta_{b\alpha}$ and $\eta_{b\beta}$. The amplitude and phase required for the space-vector modulation (SVM) stage are calculated as [44]

$$m_b = \sqrt{\eta_{b\alpha}^2 + \eta_{b\beta}^2} \tag{36}$$
$$\delta_b = \arctan(\eta_{b\alpha}, \eta_{b\beta}). \tag{37}$$

The control law (35) is nonlinear because of the state variable v_{dc} in the denominator. However, this allows compensating the dc-bus voltage variations and, in this way, low order harmonics in the grid-side VSC currents and voltages to be eliminated. These harmonics appear when a dc-bus voltage ripple with a frequency of $2\omega_s$ exists due to unbalanced grid conditions.

The technique described in [45] is used, in order to separate the sequence components of the voltage and current signals needed in the control law implementation.

REFERENCES

[1] F. M. Hughes, O. Anaya-Lara, N. Jenkins, and G. Strbac, "Control of DFIG-based wind generation for power network support," *IEEE Trans. Power Syst.*, vol. 20, no. 4, pp. 1958–1966, Nov. 2005.

[2] Integration of Large Scale Wind Generation Using HVDC and Power Electronics CIGRE, Tech. Rep. C. W. G. B4.39, Feb. 2009.

[3] J. Morren and S. W. H. de Haan, "Short-circuit current of wind turbines with doubly fed induction generator," *IEEE Trans. Energy Convers.*, vol. 22, no. 1, pp. 174–180, Mar. 2007.

[4] J. M. Mauricio, A. E. Leon, A. Gomez-Exposito, and J. A. Solsona, "An adaptive nonlinear controller for DFIM-based wind energy conversion systems," *IEEE Trans. Energy Convers.*, vol. 23, no. 4, pp. 1025–1035, Dec. 2008.

[5] J. M. Carrasco, L. G. Franquelo, J. T. Bialasiewicz, E. Galvan, R. C. P. Guisado, M. A. M. Prats, J. I. León, and N. Moreno-Alfonso, "Power-electronic systems for the grid integration of renewable energy sources: A survey," *IEEE Trans. Ind. Electron.*, vol. 53, no. 4, pp. 1002–1016, Jun. 2006.

[6] Z. Saad-Saoud, M. L. Lisboa, J. B. Ekanayake, N. Jenkins, and G. Strbac, "Application of STATCOMs to wind farms," *Proc. Inst. Elect. Eng. Generation, Transmission and Distribution*, vol. 145, pp. 511–516, Sep. 1998.

[7] H. Gaztanaga, I. Etxeberria-Otadui, S. Bacha, and D. Roye, "Fixed-speed wind farm operation improvement by using DVR devices," in *IEEE Int. Symp. Industrial Electronics (ISIE'07)*, Jun. 2007, pp. 2679–2684.

[8] A. Luna, P. Rodriguez, R. Teodorescu, and F. Blaabjerg, "Low voltage ride through strategies for SCIG wind turbines in distributed power generation systems," in *IEEE Power Electronics Specialists Conf. (PESC'08)*, Jun. 2008, pp. 2333–2339.

[9] C. Hochgraf and R. H. Lasseter, "Statcom controls for operation with unbalanced voltages," *IEEE Trans. Power Del.*, vol. 13, no. 2, pp. 538–544, Apr. 1998.

[10] H.-S. Song and K. Nam, "Dual current control scheme for PWM converter under unbalanced input voltage conditions," *IEEE Trans. Ind. Electron.*, vol. 46, no. 5, pp. 953–959, Oct. 1999.
[11] A. Yazdani and R. Iravani, "A unified dynamic model and control for the voltage-sourced converter under unbalanced grid conditions," *IEEE Trans. Power Del.*, vol. 21, no. 3, pp. 1620–1629, Jul. 2006.
[12] M. Bongiorno and J. Svensson, "Voltage dip mitigation using shunt-connected voltage source converter," *IEEE Trans. Power Electron.*, vol. 22, no. 5, pp. 1867–1874, Sep. 2007.
[13] A. E. Leon, J. M. Mauricio, J. A. Solsona, and A. Gomez-Exposito, "Software sensor-based STATCOM control under unbalanced conditions," *IEEE Trans. Power Del.*, vol. 24, no. 3, pp. 1623–1632, Jul. 2009.
[14] Y. Suh, V. Tijeras, and T. A. Lipo, "A nonlinear control of the instantaneous power in dq synchronous frame for PWM AC/DC converter under generalized unbalanced operating conditions," in *Proc. 37th IAS Annual Meeting*, Oct. 2002, vol. 2, pp. 1189–1196.
[15] R. Teodorescu, F. Blaabjerg, M. Liserre, and P. C. Loh, "Proportional-resonant controllers and filters for grid-connected voltage-source converters," *Proc. Inst. Elect. Eng., Electric Power Applications*, vol. 153, pp. 750–762, Sep. 2006.
[16] G. Escobar, P. Mattavelli, A. M. Stankovic, A. A. Valdez, and J. Leyva-Ramos, "An adaptive control for UPS to compensate unbalance and harmonic distortion using a combined capacitor/load current sensing," *IEEE Trans. Ind. Electron.*, vol. 54, no. 2, pp. 839–847, Apr. 2007.
[17] Y. Suh and T. A. Lipo, "Modeling and analysis of instantaneous active and reactive power for PWM AC/DC converter under generalized unbalanced network," *IEEE Trans. Power Del.*, vol. 21, no. 3, pp. 1530–1540, Jul. 2006.
[18] J. Hu and Y. He, "Modeling and control of grid-connected voltage-sourced converters under generalized unbalanced operation conditions," *IEEE Trans. Energy Convers.*, vol. 23, no. 3, pp. 903–913, Sep. 2008.
[19] S. M. Dehghan, M. Mohamadian, and A. Y. Varjani, "A new variable-speed wind energy conversion system using permanent-magnet synchronous generator and z-source inverter," *IEEE Trans. Energy Convers.*, vol. 24, no. 3, pp. 714–724, Sep. 2009.
[20] M. Chinchilla, S. Arnaltes, and J. C. Burgos, "Control of permanent-magnet generators applied to variable-speed wind-energy systems connected to the grid," *IEEE Trans. Energy Convers.*, vol. 21, no. 1, pp. 130–135, Mar. 2006.
[21] S. M. Muyeen, R. Takahashi, T. Murata, and J. Tamura, "Integration of an energy capacitor system with a variable-speed wind generator," *IEEE Trans. Energy Convers.*, vol. 24, no. 3, pp. 740–749, Sep. 2009.
[22] A. Mullane, G. Lightbody, and R. Yacamini, "Wind-turbine fault ride-through enhancement," *IEEE Trans. Power Syst.*, vol. 20, no. 4, pp. 1929–1937, Nov. 2005.
[23] W. Hu, Z. Chen, Y. Wang, and Z. Wang, "Flicker mitigation by active power control of variable-speed wind turbines with full-scale back-to-back power converters," *IEEE Trans. Energy Convers.*, vol. 24, no. 3, pp. 640–649, Sep. 2009.
[24] T. Senjyu, S. Tamaki, E. Muhando, N. Urasaki, H. Kinjo, T. Funabashi, H. Fujita, and H. Sekine, "Wind velocity and rotor position sensorless maximum power point tracking control for wind generation system," *Renewable Energy*, vol. 31, pp. 1764–1775, Sep. 2006.
[25] G. Saccomando, J. Svensson, and A. Sannino, "Improving voltage disturbance rejection for variable-speed wind turbines," *IEEE Trans. Energy Convers.*, vol. 17, no. 3, pp. 422–428, Sep. 2002.
[26] C. H. Ng, L. Ran, and J. Bumby, "Unbalanced-grid-fault ride-through control for a wind turbine inverter," *IEEE Trans. Ind. Appl.*, vol. 44, no. 3, pp. 845–856, May/Jun. 2008.
[27] S. K. Salman and A. L. J. Teo, "Windmill modeling consideration and factors influencing the stability of a grid-connected wind power-based embedded generator," *IEEE Trans. Power Syst.*, vol. 18, no. 2, pp. 793–802, May 2003.
[28] S. Huang, X. Long, L. Cai, K. Huang, and J. Gao, "An engineering design of a 2MW direct-drive permanent-magnet wind-power generation system," in *Int. Conf. Electrical Machines and Systems, 2008 (ICEMS 2008)*, Oct. 2008, pp. 2337–2342.
[29] A. Yazdani and R. Iravani, "A generalized state-space averaged model of the three-level NPC converter for systematic DC-voltage-balancer and current-controller design," *IEEE Trans. Power Del.*, vol. 20, no. 2, pt. 1, pp. 1105–1114, Apr. 2005.
[30] V. Blasco and V. Kaura, "A new mathematical model and control of a three-phase AC-DC voltage source converter," *IEEE Trans. Power Electron.*, vol. 12, no. 1, pp. 116–123, Jan. 1997.
[31] P. Rioual, H. Pouliquen, and J.-P. Louis, "Regulation of a PWM rectifier in the unbalanced network state using a generalized model," *IEEE Trans. Power Electron.*, vol. 11, no. 3, pp. 495–502, May 1996.
[32] B. Blazic and I. Papic, "Improved D-StatCom control for operation with unbalanced currents and voltages," *IEEE Trans. Power Del.*, vol. 21, no. 1, pp. 225–233, Jan. 2006.
[33] R. S. Pena, R. J. Cardenas, J. C. Clare, and G. M. Asher, "Control strategies for voltage control of a boost type PWM converter," in *Proc. IEEE 32nd Power Elec. Spec. Conf. (PESC'01)*, Jun. 2001, vol. 2, pp. 730–735.
[34] G. Tsourakis, B. M. Nomikos, and C. D. Vournas, "Contribution of doubly fed wind generators to oscillation damping," *IEEE Trans. Energy Convers.*, vol. 24, no. 3, pp. 783–791, Sep. 2009.
[35] Y. Mishra, S. Mishra, M. Tripathy, N. Senroy, and Z. Y. Dong, "Improving stability of a DFIG-based wind power system with tuned damping controller," *IEEE Trans. Energy Convers.*, vol. 24, no. 3, pp. 650–660, Sep. 2009.
[36] N. R. Ullah, K. Bhattacharya, and T. Thiringer, "Wind farms as reactive power ancillary service providers-technical and economic issues," *IEEE Trans. Energy Convers.*, vol. 24, no. 3, pp. 661–672, Sep. 2009.
[37] I. Erlich and U. Bachmann, "Grid code requirements concerning connection and operation of wind turbines in Germany," in *Proc. IEEE Power Engineering Society General Meeting*, Jun. 2005, vol. 2, pp. 1253–1257.
[38] Red Eléctrica P.O. 12.3, Requisitos de respuesta frente a huecos de tensión de las instalaciones de producción en régimen especial. Spanish regulations (in Spanish) Spanish Ministery of Industry, Turism and Commerce, BOE Núm. 254., Oct. 2006, pp. 1–7 [Online]. Available: www.ree.es
[39] J. Slootweg, S. de Haan, H. Polinder, and W. Kling, "General model for representing variable speed wind turbines in power system dynamics simulations," *IEEE Trans. Power Syst.*, vol. 18, no. 1, pp. 144–151, Feb. 2003.
[40] E. Koutroulis and K. Kalaitzakis, "Design of a maximum power tracking system for wind-energy-conversion applications," *IEEE Trans. Ind. Electron.*, vol. 53, no. 2, pp. 486–494, Apr. 2006.
[41] V. Agarwal, R. Aggarwal, P. Patidar, and C. Patki, "A novel scheme for rapid tracking of maximum power point in wind energy generation systems," *IEEE Trans. Energy Convers.*, vol. 25, no. 1, pp. 228–236, Mar. 2010.
[42] H. Akagi, Y. Kanazawa, and A. Nabae, "Instantaneous reactive power compensators comprising switching devices without energy storage components," *IEEE Trans. Ind. Appl.*, vol. 20, no. 3, pp. 625–630, May/Jun. 1984.
[43] W. Bierbooms, "A gust model for wind turbine design," *JSME Int. J.*, ser. B Fluids and Thermal Engineering, vol. 47, no. 2, pp. 378–386, 2004.
[44] M. Saeedifard, H. Nikkhajoei, and R. Iravani, "A space vector modulated STATCOM based on a three-level neutral point clamped converter," *IEEE Trans. Power Deliv.*, vol. 22, no. 2, pp. 1029–1039, Apr. 2007.
[45] H.-S. Song, I.-W. Joo, and K. Nam, "Source voltage sensorless estimation scheme for PWM rectifiers under unbalanced conditions," *IEEE Trans. Ind. Electron.*, vol. 50, no. 6, pp. 1238–1245, Dec. 2003.

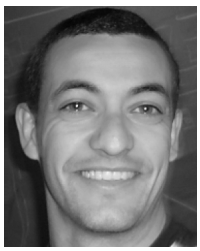

Andres E. Leon (S'05) was born in Argentina, in 1979. He received the electrical engineering degree from the National University of Comahue, Neuquén, Argentina, in 2005. He is currently working toward the Ph.D. degree in control systems at the Instituto de Investigaciones en Ingeniería Eléctrica "Alfredo Desages" (IIIE), Universidad Nacional del Sur, Bahía Blanca, Argentina.

His primary areas of interest are power systems control, custom power systems, and wind energy conversion systems.

Juan Manuel Mauricio (S'01) was born in Argentina, in 1977. He received the electrical engineering degree from the National University of Comahue, Neuquén, Argentina, in 2003. He received the master and doctor engineering degrees from the University of Seville of Spain, in 2007 and 2009, respectively.

Since 2004, he has been with the Department of Electrical Engineering, University of Seville, where he is currently an Assistant Professor. His primary areas of interest are power systems and electrical machines modeling and control, renewable energy generation, voltage source converters based applications, and electrical vehicles.

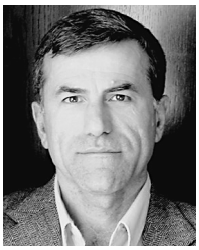

Antonio Gómez-Expósito (M'87–SM'95–F'05) received the electrical engineering and doctor degrees from the University of Seville, Spain.

Since 1982, he has been with the Department of Electrical Engineering, University of Seville, where he is currently a Professor and Chairman of the department. He is also directing the recently created Endesa Red Chair. His primary areas of interest are optimal power system operation, state estimation, digital signal processing, and control of flexible ac transmission system devices.

Jorge Alberto Solsona (S'94–M'97–SM'04) received the electronics engineer and Dr. degrees from the Universidad Nacional de La Plata, La Plata, Argentina, in 1986 and 1995, respectively.

Currently, he is with the Instituto de Investigaciones en Ingeniería Eléctrica Alfredo Desages (IIIE), Departamento de Ingeniería Eléctrica y de Computadoras, Universidad Nacional del Sur, Bahía Blanca, Argentina, and CONICET where he is involved in teaching and research on control theory and its applications to electromechanical systems.